

Article

Glacial Erosion Rates Determined at Vorab Glacier: Implications for the Evolution of Limestone Plateaus

Olivia Steinemann ^{1,*}, Alicia Martinez ², Vincenzo Picotti ², Christof Vockenhuber ¹ and Susan Ivy-Ochs ^{1,2}

¹ Laboratory of Ion Beam Physics, ETH Zürich, Otto-Stern-Weg 5, 8093 Zürich, Switzerland; cvockenh@ethz.ch (C.V.); ivy@ethz.ch (S.I.-O.)

² Geological Institute, ETH Zürich, Sonneggstr. 5, 8092 Zürich, Switzerland; alicia.c.martinez.v@gmail.com (A.M.); vincenzo.picotti@erdw.ethz.ch (V.P.)

* Correspondence: okronig@phys.ethz.ch

Abstract: Understanding how fast glaciers erode their bedrock substrate is one of the key elements in reconstructing how the action of glaciers gives mountain ranges their shape. By combining cosmogenic nuclide concentrations determined in glacially abraded bedrock with a numerical model, we quantify glacial erosion rates over the last 15 ka. We measured cosmogenic ³⁶Cl in fourteen samples from the limestone forefield of the Vorab glacier (Eastern Alps, Switzerland). Determined glacial erosion rates range from 0.01 mm a⁻¹ to 0.16 mm a⁻¹. These glacial abrasion rates differ quite markedly from rates measured on crystalline bedrock (>1 mm a⁻¹), but are similarly low to the rates determined on the only examined limestone plateau so far, the Tsanfleuron glacier forefield. Our data, congruent with field observations, suggest that the Vorab glacier planed off crystalline rock (Permian Verrucano) overlying the Glarus thrust. Upon reaching the underlying strongly karstified limestone the glacier virtually stopped eroding its bed. We attribute this to immediate drainage of meltwater into the karst passages below the glacier, which inhibits sliding. The determined glacial erosion rates underscore the relationship between geology and the resulting landscape that evolves, whether high elevation plateaus in limestone terrains or steep-walled valleys in granitic/ gneissic areas.

Keywords: glacial erosion rates; cosmogenic ³⁶Cl; Swiss Alps; limestone plateau; Bündnerbergjoch



Citation: Steinemann, O.; Martinez, A.; Picotti, V.; Vockenhuber, C.; Ivy-Ochs, S. Glacial Erosion Rates Determined at Vorab Glacier: Implications for the Evolution of Limestone Plateaus. *Geosciences* **2021**, *11*, 356. <https://doi.org/10.3390/geosciences11090356>

Academic Editors: Roger Urgeles Esclasans and Jesús Martínez-Frías

Received: 30 June 2021

Accepted: 20 August 2021

Published: 24 August 2021

Publisher's Note: MDPI stays neutral with regard to jurisdictional claims in published maps and institutional affiliations.



Copyright: © 2021 by the authors. Licensee MDPI, Basel, Switzerland. This article is an open access article distributed under the terms and conditions of the Creative Commons Attribution (CC BY) license (<https://creativecommons.org/licenses/by/4.0/>).

1. Introduction

Many valleys and overdeepenings in forelands are the result of (sub) glacial erosion [1–7]. During the Quaternary, powerful ice masses were the main drivers in sculpting the Alpine landscape by bedrock erosion and production of large amounts of sediment [8–10]. Because there are numerous geological (e.g., lithology, structural geology, fractures and faults, amount of sediment) and glaciological factors (ice thickness, slope, orientation) that influence the rate of glacial erosion ([11,12] and references therein), and direct measurements are nearly impossible, knowledge about how fast glaciers are able to erode their underlying surface is still remarkably limited.

Over the previous century, different direct and indirect scientific approaches have been performed to determine subglacial erosion rates. In the past, researchers focused more on direct measurements [13,14] at the bedrock–ice interface or sediment yield measurements in meltwater streams [15–17]. Modern research concentrates more on numerical models based on glacier dynamics [18–22]. In the last decades, cosmogenic nuclide techniques have been shown to offer a unique possibility of determining glacial erosion rates directly on freshly exposed, glacially polished surfaces [23–26]. If two different cosmogenic nuclides (¹⁰Be/²⁶Al or ¹⁰Be/in-situ ¹⁴C) are combined, this can even allow the possibility of determining the duration of the latest glacial burial history and, if glacial erosion was relatively small (e.g., marginal positions or beneath cold-based glaciers), it gives evidence on the glacial erosion rates [26]. If only one cosmogenic nuclide can be used, an independent archive to constrain the burial history of the sampled site is needed to determine the rate

of glacial erosion [25]. This method, implementing cosmogenic ^{36}Cl , has the advantage of not being restricted to quartz-bearing lithologies (e.g., granites) but also allows the determination of glacial erosion rates on carbonates. In this study at Tsanfleuron glacier (Figure 1) [26], strikingly low glacial erosion rates (<0.08 mm/a) were determined on the flat-lying massive limestone bedrock.

In this study, we apply the method of using one cosmogenic nuclide, specifically ^{36}Cl , to measure how rapidly the Vorab glacier (Switzerland) erodes the underlying limestone bed. The fortuitous presence of the famous Glarus thrust allows the study of how a glacier responds when transitioning from an easy-to-erode rock, such as Permian schists, to a difficult-to-erode rock, such as limestone (cf. [25,26]). We examine some of the hypotheses presented in [25], in which we focussed on the Tsanfleuron glacier limestone forefield (Figure 1). Our results from the Vorab glacier site, in addition to providing direct measurements of how fast glaciers erode, also contribute to increasing the still vague understanding of how the high-elevation, low-relief limestone plateaus in the Alps have formed and persisted through numerous large-scale glaciations.

2. Study Area

Focus of the study is a high-elevated (2600 m a.s.l.), low-relief area located within the Little Ice Age (LIA) extent of the Vorab glacier, on the border between the political regions (cantons) of Glarus and Grisons in eastern Switzerland (Figure 1). The west-facing glacier (Figures 1 and 2) with a surface area of 1.20 km² (year 2014, [27]) stretches between the Bündler Vorab (3028 m a.s.l.) and the Gletscherhorn (2804 m a.s.l.). During the LIA, it covered an area of 3.3 km² (Figure 2). During this time, the northern part of the glacier flowed down over the almost 400 m high, nearly vertical cliff to Glarus to the north, whereas the southern part extended about 1.7 km further southward than its present-day position, on a gently increasingly steep slope dipping towards the Grisons side. Ever since, the glacier has been retreating, with few years of stagnation or small brief advances [27]. A selection of glacier extents of different years, illustrated in Figure 2, shows the retreat history of the Vorab glacier.

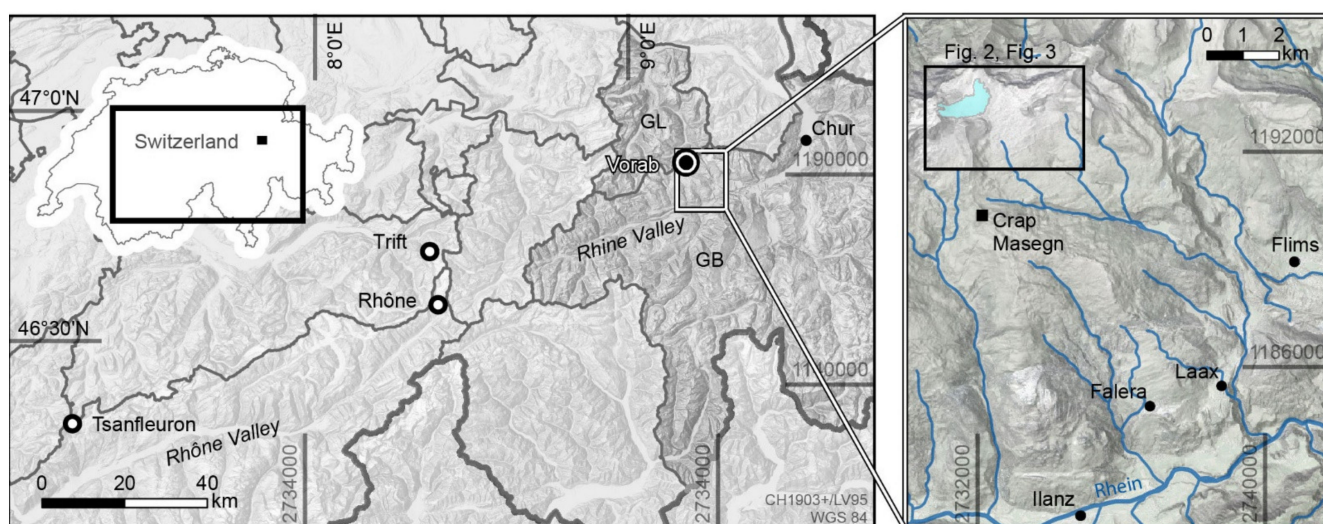


Figure 1. Overview maps. **Left:** Location of the Vorab glacier (black point) west of Chur at the border between the canton of Glarus (GL) and Grisons (GB). Extent of the map within Switzerland is indicated by the black rectangle on the inset map. Other locations, in the Swiss Alps, where glacial erosion rates were determined using cosmogenic nuclides are indicated as white points. **Right:** close-up of the study site area, with the Vorab glacier extent (2019) in light blue and the location of the weather station at Crap Masegn. The black rectangle shows the extent of Figures 2 and 3. Background maps and outlines of the cantons are reproduced with the authorization of the Swiss Federal Office of Topography (swisstopo).

Because of its unique geology, the area is part of the UNESCO World Heritage Tectonic Arena Sardona [28,29]. At several locations around the glacier front and likely also still below the glacier, the famous Glarus thrust plane [30,31] is exposed (Figure 2), where older (Permian) nappes overlie younger (lower Cretaceous) carbonates. In the study area, the Cretaceous carbonates are covering most of the glacier forefield. The area inside of the LIA extent is dominated by massive limestone beds and by siliceous limestone outside of the LIA extent (Figure 2). The hanging wall of the Glarus thrust is mainly composed of Permian Verrucano, visible as high peaks in the surrounding of the Vorab glacier (Gletscherhorn 2804 m a.s.l., Glarner Vorab 3018 m a.s.l. Bündner Vorab 3028 m a.s.l. and Laaxer Stöckli 2899 m a.s.l.).

During winter months the area is a ski resort (Flims-Laax-Falera, Figure 1), including the Vorab glacier itself. This is why certain areas in and outside the LIA extents were strongly affected and artificially modified, which has to be kept in mind during geomorphological mapping and interpretation.

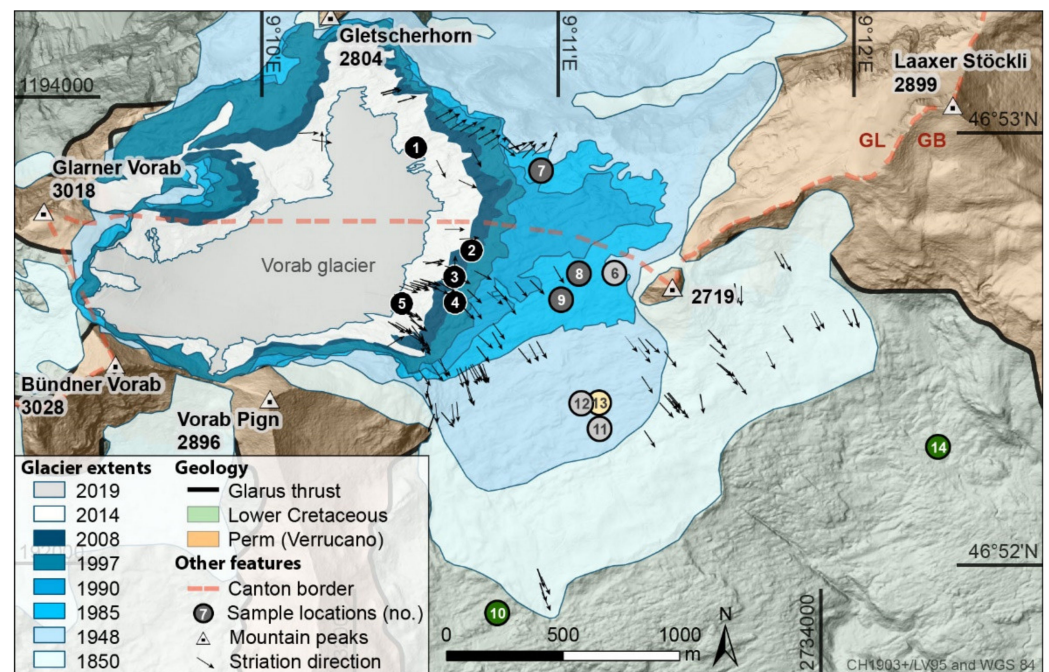


Figure 2. Geological map combined with the chronology of past glacier extents since the LIA. Circles show the location and number of the samples taken for ^{36}Cl analysis. Bedrock samples are grouped according to their position relative to the glacier extents: green: outside LIA extent (1850), light grey: inside 1948, dark grey: inside 1985, black: 2018; the only sampled boulder (Vorab-13) is yellow. Background map, geology and glacier extents are based on the swissAlti3D 2019, the geological 1:500,000 map and the topographic maps of the different years, reproduced with the authorization of the Swiss Federal Office of Topography (swisstopo). For location of the map see Figure 1.

3. Materials and Methods

3.1. Fieldwork

Fieldwork in the forefield of the Vorab glacier was restricted to the summer months in 2018, because of the continued presence of snow from the previous winter. Major focus was put on the geomorphology, e.g., the glacial landforms and deposits (moraine ridges, sediment stripes, striations). The area was mapped on a topographic map (1:10,000) supported by a tablet with GIS software (GIS Pro, Grafa 2014) that allowed to directly save striation measurements and the locations of mapped features, photographs and notes as layer files. The manually and digitally collected data, including knowledge from historical maps, were evaluated and combined to create a geomorphological map.

A total of 14 samples were taken for cosmogenic ^{36}Cl analysis (Figure 2). Eleven samples were collected from inside the LIA extent. We divided these into three sub-groups depending on their location relative to present and past ice margin positions (see Figure 2): (i) just in front of the 2018 glacier extent (Vorab-1-Vorab-5), (ii) near the extent of the glacier around 1985 (Vorab-7-Vorab-9), (iii) near the extent of the glacier of 1948 (Vorab-6, Vorab-11 and Vorab-12). Two samples were taken outside of the LIA extent (Vorab-10, Vorab-14). One sample (Vorab-13) was taken on a boulder located inside the LIA extent just next to Vorab-12. Only glacially polished surfaces were sampled, where clear striations were visible. Plucked areas were strictly avoided. An elevated location of the sample compared to its surrounding was favourable, to avoid shielding through micro topography. Additionally, it lowered the duration of snow cover due to frequent winds. About 500 g of the top few centimetres (<5 cm) were extracted with a battery-operated saw, hammer and chisel. The exact location of the sample, sample thickness, dip and dip direction and the topographic shielding were measured on site using a compass and clinometer.

3.2. ^{36}Cl Sample Preparation

Samples were crushed with a hydraulic press and sieved to a grain size of <400 μm . After leaching the samples in a weak HNO_3 solution, an aliquot of dried sample material (10 g) was sent to Actlabs S.A. (Ancaster, ON, Canada) to determine the composition of major and trace elements with ICP-MS (inductively coupled plasma mass spectrometry) (Table 1). Following this, ^{36}Cl sample preparation was undertaken at ETH Zürich (Laboratory of Ion Beam Physics) according to the sample preparation described by [32,33]. ^{36}Cl and total Cl concentrations were measured by AMS (accelerator mass spectrometry) (Tables 1 and 2) performed with the 6 MV TANDEM system at the Laboratory of Ion Beam Physics, ETH Zürich. Sample ratios were measured against the standard material K382/4N with a $^{36}\text{Cl}/\text{Cl}$ value of 17.36×10^{-12} [34]. The apparent exposure ages were calculated with an in-house MATLAB code (Table 2) using equations and constants described in [35] and the following ^{36}Cl production rates: a spallogenic production rate of calcium of $48.8 \pm 3.4 \text{ atoms g}_{\text{Ca}}^{-1} \text{ a}^{-1}$, $5.3 \pm 1.0 \text{ }^{36}\text{Cl} \text{ atoms g}_{\text{Ca}}^{-1} \text{ a}^{-1}$ for muon capture in calcium and a neutron capture rate of $760 \pm 150 \text{ neutrons g}_{\text{air}}^{-1}$. All production pathways were accounted for in the code (see also [23]).

3.3. MECED Model

The MECED model was programmed by C. Wirsig and V. Alfimov [23,35], then modified by O. Steinemann [25]. The code is based on equations, production rates and constants described in [35]. Additional input parameters are a glacier fluctuation history, i.e., when the sample location was covered by a glacier (no ^{36}Cl production) or was ice free (^{36}Cl production), and potential snow coverage (snow depth and duration in months), as well as the karst weathering rate during ice-free periods. The latter two lead to a reduced final ^{36}Cl concentration; the present maximal thickness of the Vorab glacier is 60–80 m (27). The glacier was thicker during the LIA and similar during late Holocene glacier advances. Production of ^{36}Cl , including production by muons, through this thickness of ice is 0.02–0.04% of total production on a fully exposed, ice-free surface. Already with an ice thickness of only 5 m, e.g., in marginal position, production is <5%.

With these inputs, the model gives two main outputs. The first is a sample specific diagram of ^{36}Cl concentration evolution over time based on the glacial fluctuation history (also see Section 5.2.1) including the final modelled (theoretical) nuclide concentration. This indicates what the concentration should be at that specific sample location presently with the used glacial fluctuation history, snow coverage input and karst weathering rate. The second output is a corresponding depth vs. concentration plot, showing the decrease of the ^{36}Cl concentration with depth into the limestone bedrock. By intersecting this modelled concentration-depth profile with the actual AMS measured ^{36}Cl concentration for that sample, one can determine how much of the bedrock surface must have been removed by the glacier at that specific sample location. By dividing this erosion depth by the total time

of glacier coverage (glacier fluctuation history input), the glacial erosion rate is calculated. Detailed description of the MECED model and a thorough discussion of the influencing factors and limitations can be found in [36,37].

4. Overview of Geomorphology of Vorab Glacier Forefield

The most important observations made during the fieldwork will be described shortly; in this section the focus will be on glacial features such as moraine deposits, sediment stripes and striations. In the following section karst and bedrock features, such as bedrock steps, erosional channels and swallow holes will be described. An overview of the identified landforms and their apparent exposure ages is illustrated in the geomorphological map (Figure 3).

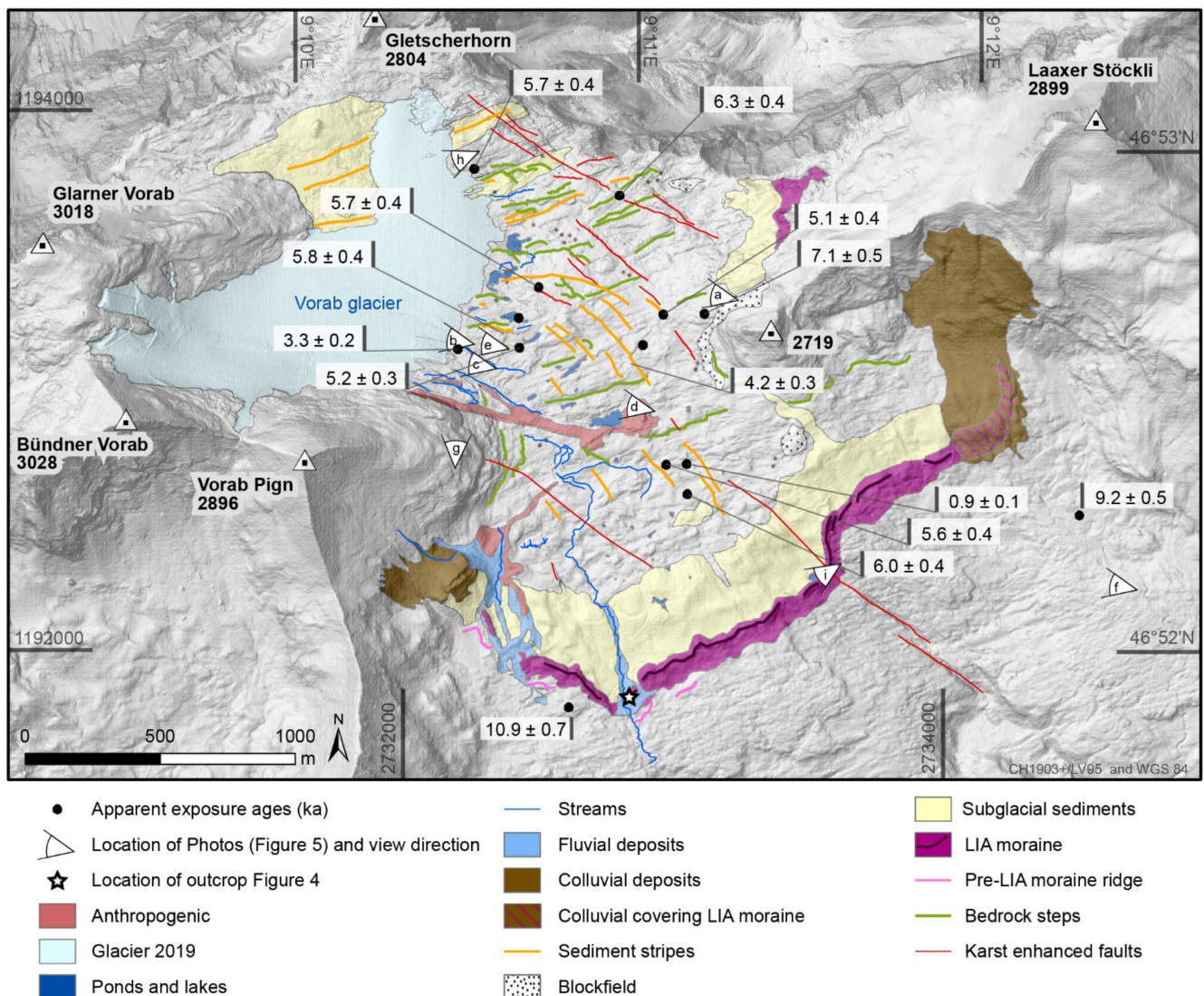


Figure 3. Geomorphological map of the Vorab glacier forefield showing the mapped features and the apparent ^{36}Cl exposure ages. Star shows the location of the described sedimentary outcrop (Figure 4). For location of the map see Figure 1.

4.1. Glacial Landforms and Sediments

The LIA margins were designated through field observations and according to the topographic map of 1895 [38], along with orthophoto and hillshade maps [39]. The largest, most continuous LIA moraine ridge is approximately 1 km long and up to 15 m high (Figure 3). The northernmost LIA moraine fragment has a length of about 200 m. These

LIA moraine ridges are not vegetated (or only patchily) and consist of angular clasts in a sandy to fine-grained matrix. Most large fragments (up to 15 cm) consist of Verrucano, larger components (0.5–1 m) are mainly limestones and angular. There are a few locations, especially in the northern moraine fragment, where larger Verrucano fragments are found more frequently.

The main meltwater stream crosscuts the LIA moraine in the southwest, creating a 2 m high and 6 m wide natural outcrop (Figures 3 and 4a). After the outcrop was cleaned with a shovel it was sketched in detail (Figure 4b) as described in [40] using the abbreviations from [41]. This investigation revealed the pushing and the gravitational reworking of sediment at the glacier front during the LIA because the folds show a clear forward movement toward the south. There is a wide variability in the size and lithology of the clasts. In the Dms (diamicton, matrix-supported, stratified) that clearly dominates the outcrop, there are interbedded layers that were deposited episodically (Figure 4b). These vary from clast-dominated layers of several centimetres thick that were deposited during periods of stronger energy and higher water flow to layers of very fine sand that were probably deposited during quieter periods. A repetitive sequence was not recognised. At the outermost edge, there is a hill structure consisting of GSc (clast-supported gravel and sand), which could be a remnant of a buried moraine (Figure 4b).

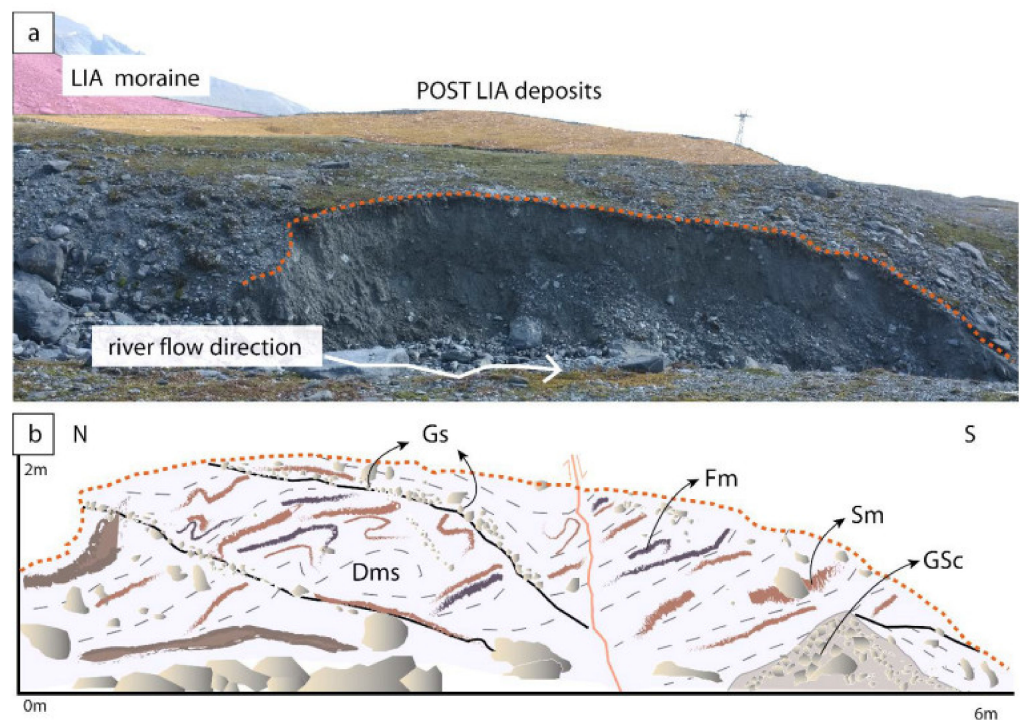


Figure 4. Photograph (a) and interpretation (b) of a river-cut outcrop through the LIA margin deposits. The interpretation shows that the advancing LIA glacier pushed the sediments. Dms: diamicton completely unsorted, matrix-supported, stratified, Gs: gravel stratified, Fm: fines massive, Sm: sand massive, GSc: gravel, sand, clast-supported [41]. LIA moraine coloured pink in the photograph, post-LIA deposits coloured in orange. See Figure 3 for location of the outcrop.

In contrast to the area just inside of the LIA moraine ridge, where secondary postglacial debris was deposited through fluvial and ice decay processes with a relatively fresh appearance, the pre-LIA moraines (outside LIA) are already strongly vegetated, and soil formation has started. These older moraines form clear 1–2 m high hills tens to hundreds of meters distal to the LIA moraines (Figure 3). The post-LIA moraines were recognized as elevated sediment accumulations, maximally 1 m high, perpendicular to the striation direction, which indicates formation of the material by the glacier. These faint ridges are

mainly composed of cm- to dm-sized clast and very little matrix. It is noteworthy that the glacier forefield has no to very sparse subglacial till cover (Figure 5a), and if there are till deposits, for example just inside of the LIA moraines (Figure 5i), it lacks a fine matrix. However, some faint flute structures were observed.

In the forefield of the Vorab glacier, sediment stripes in different dimensions ranging from a few tens of centimetres up to several meters in width (Figure 5b,c) were observed and mapped (Figure 3). The clast size ranges from centimetre- up to metre-sized. It is striking that in the south-western part of the glacier forefield, the sediment stripes consist of much smaller and finer clasts; those in the north and northeast show larger as well as finer angular clasts. Based on field investigations, it can be concluded that these sediments were transported englacially; as Figure 5b shows, they emerged from within the ice and were not transported subglacially. As the glacier melts, the sediment remains. The trend of individual stripes is more or less straight, crossing over highs and lows in topography, indicating that they are not related to meltwater processes. Accordingly, they are excellent indicators of past ice-flow directions [25].

Over 200 striations were measured in the glacier forefield and are portrayed in Figure 2; an example is shown in Figure 5d. Most were measured on horizontal polished bedrock surfaces, where these typical glacier scratch marks could be seen easily. Others were measured based on the orientation of recrystallized calcite fibres formed on the lee side of small bedrock irregularities. Clearly, the glacier had two main directions; the more obvious one starting towards east and turning south. In the northern part, however, the traces point northwards, towards Glarus (Figures 1 and 2). In the centre, striations point toward the southeast, potentially locating the former ice divide. No crosscutting striations or other evidence was found that would indicate a recent change in ice-flow direction. The presence of fresh striations and the measured southerly direction on the southern side of the Verrucano ridge (between the 2719 m a.s.l. peak and the Laaxer Stöckli (Figure 3)) suggests that the glacier at least in part overtopped this ridge, as shown also by the historical maps (Figure 2). Outside the LIA moraine, no striations can be observed.

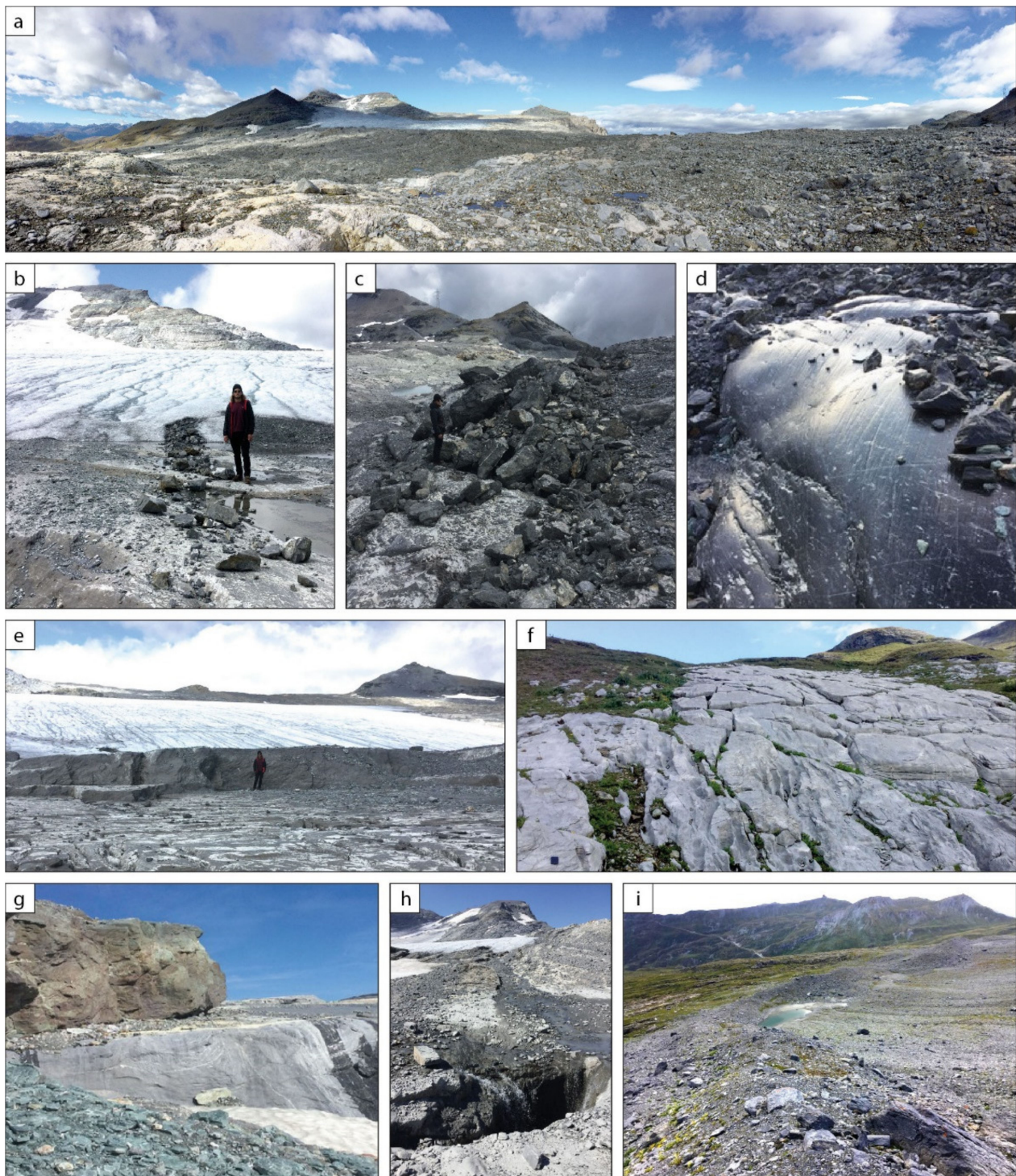


Figure 5. Photo panel, location of each photo and view direction is shown on Figure 3. (a) View across the flat limestone forefield of the Vorab glacier (in the background). Note the sparse sediment cover. (b) Sediment stripe with small clasts emerging englacially. (c) Sediment stripe with large clasts, see person for scale. (d) Polished and striated bedrock. (e) Bedrock step in front of the Vorab glacier, see person for scale. (f) Strongly karstified bedrock with deep channels and karren outside of the LIA extent. (g) Glarus thrust with Verrucano (phyllites) on top of Lower Cretaceous limestone. (h) Swallow hole where glacial meltwater disappears into the karst system. (i) LIA moraine ridge.

4.2. Bedrock, Karst and Hydrological Features

Bedrock steps are frequent features in the limestone forefield of the Vorab glacier. The steps are up to 5 m high and several are 100 m long (Figure 5e). In between the steps, which can be several meters apart, the surfaces are smooth and flat with an average dip of few degrees toward the southeast. Similar stepped limestone landforms have been described in the literature [42,43].

Karst weathering is an important factor influencing the appearance of the limestone, and it is also a significant parameter with respect to the modelling and calculation of the glacial erosion rates (see Section 5.2.1). Based on the presence and absence of glacial striations in the glacier forefield it can be concluded that the intensity varies across the limestone forefield. Striations were mainly observed on elevated crests of the bedrock, indicating that at these locations karst weathering rates have been rather low since the location was exposed. This is in contrast to the depressions and channels in between these local elevation highs. There the water has already found its way through the rock, often forming several dm-deep (subglacial) channels. These channels mainly follow the direction of the bedrock faults. Very few lie along the previously mentioned bedrock steps. At present, in spring and early summer, great amounts of meltwater flow out to the glacier forefield. Some of the meltwater is redirected through artificial pipes to prevent damage to infrastructure, like the gravel road. However, in many areas the (melt-)water disappears into swallow holes, especially in the north-western part of the glacier forefield (Figure 5h). Field observations indicate there are several metres-deep shafts and it is presumed that these connect to an extensive karst network, as has been shown to be the case in the Flims area just to the east [44]. Other swallow holes are filled with finer sediments, so little or no water seeps through and seasonal lakelets form. Further meltwater lakes have formed in bedrock depressions. The size of the lakes ranges from 2 to 20 m² and they often have sandy-silty material on the ground and on the lake shores. Sometimes the ponds have superficial water in- and outlets. However, in most cases these superficial water streams are short and disappear into swallow holes, highlighting the very efficient karst drainage system. Outside of the LIA moraine ridges, water and creeks are less common, but the bedrock outcrops are strongly crossed by karren fields, which can be several meters deep (Figure 5f).

5. Glacial Erosion Rate Determinations

5.1. "Apparent" Exposure Ages

The AMS-measured ³⁶Cl concentrations and the apparent exposure ages calculated from them are shown in Table 1 and are plotted on the map of Figure 3. The ages listed in Table 1 are corrected for neither karst weathering erosion nor for snow cover, because they will not be used for chronological interpretations. The apparent exposure ages range from 3.3 ± 0.2 ka (Vorab-5) to 10.9 ± 0.7 ka (Vorab-10) excluding the boulder sample Vorab-13 with an exposure age of 0.9 ± 0.1 ka.

The samples located outside the LIA extent (Figures 2 and 3) Vorab-10 (10.9 ± 0.7 ka) and Vorab-14 (9.2 ± 0.5 ka) gave the oldest apparent exposure ages and conform relatively well to their presumable true exposure age, assuming they were last covered by the Egesen stadial glacier (12.7–11.5 ka). However, as shown in Figure 6, if snow cover and karst weathering were taken into account the modelled nuclide concentrations after 11.5 ka of exposure would be lower than the measured values (dashed green line in Figure 6a). Therefore, it seems likely that these samples were already exposed during the Bølling/Allerød (B/A) interstadial so that the bedrock surfaces could accumulate enough nuclides to account for the reduction or loss caused by the snow coverage and karst weathering. Including snow and karst correction, these ages are 13.1 ± 0.8 ka (Vorab-10) and 11.1 ± 0.6 ka (Vorab-14). These ages are in good agreement with the timing of the end of the Egesen stadial in the Alps at 11.7 ka, suggesting that excess ³⁶Cl from exposure prior to the last glacial maximum (LGM) is minimal. This question was explored in detail in the study at Tsanfleuron glacier using the same methodology [25]. There, a sample in a

cave 6 m below the glacially polished surface had less than 2% of the surface concentration, in agreement with the muon-derived concentration in the calculated depth profile (see Figure 5 in [25]). Inheritance from before the LGM at Tsanfleuron was negligible. Although the same test was not performed at Vorab, the huge thickness of ice at Vorab (estimated to be several hundred meters) during the LGM [21,22] would, in principle, have similarly removed more than 2 m of bedrock and removed nearly all previously produced ^{36}Cl .

Table 1. Sample site information, AMS-measured ^{36}Cl concentrations and calculated apparent exposure ages.

Sample	Location	Latitude	Longitude	Elevation	Thickness	Topographic Shielding	^{36}Cl Concentration	Apparent Exposure Age
							^{1,2}	
WGS 84			m a.s.l.	cm	10 ⁶ at/g		ka	
Vorab-1	2018	46.882	9.174	2653	2.5	0.9986	0.89 ± 0.05	5.7 ± 0.4
Vorab-2	2018	46.878	9.177	2635	1.0	0.9991	0.84 ± 0.05 *	5.7 ± 0.4
Vorab-3	2018	46.877	9.176	2639	2.0	0.9987	0.91 ± 0.05	5.8 ± 0.4
Vorab-4	2018	46.876	9.176	2618	1.5	0.9979	0.81 ± 0.03 *	5.2 ± 0.3
Vorab-5	2018	46.876	9.173	2640	3.0	0.9963	0.50 ± 0.03	3.3 ± 0.2
Vorab-6	1948	46.877	9.185	2623	1.5	0.9977	1.12 ± 0.06	7.1 ± 0.5
Vorab-7	1985	46.881	9.181	2616	2.0	0.9991	0.96 ± 0.05	6.3 ± 0.4
Vorab-8	1985	46.877	9.183	2609	1.5	0.9991	0.78 ± 0.05 *	5.1 ± 0.4
Vorab-9	1985	46.876	9.182	2600	1.5	0.9990	0.58 ± 0.03 *	4.2 ± 0.3
Vorab-10	outside LIA	46.864	9.178	2439	2.0	0.9962	1.26 ± 0.07	10.9 ± 0.7
Vorab-11	1948	46.871	9.184	2524	2.0	0.9988	0.77 ± 0.05 *	6.0 ± 0.4
Vorab-12	1948	46.872	9.183	2531	3.0	0.9985	0.80 ± 0.05	5.6 ± 0.4
Vorab-13	boulder	46.872	9.184	2540	6.0	0.9955	0.10 ± 0.01 *	0.9 ± 0.1
Vorab-14	outside LIA	46.870	9.203	2397	2.0	0.9955	1.23 ± 0.04 *	9.2 ± 0.5

¹ Measured against standard K382/4N (17.36 ± 0.35) $\times 10^{-12}$ [34,45]. ² Corrected for processed blank of $(1.2 \pm 0.7) \times 10^{-15}$ or $(2.1 \pm 0.4) \times 10^{-15}$ if sample is marked with a *.

Table 2. Elemental composition of leached samples. Cl values are from AMS measurements.

Sample	Al ₂ O ₃ %	CaO %	Fe ₂ O ₃ %	K ₂ O %	MgO %	MnO %	Na ₂ O %	P ₂ O ₅ %	SiO ₂ %	TiO ₂ %	Sm ppm	Gd ppm	U ppm	Th ppm	Cl ppm
Vorab-1	0.73	53.53	0.57	0.19	0.63	0.01	0.05	0.06	2.73	0.03	0.6	0.5	0.4	0.7	2.83 ± 0.08
Vorab-2	0.44	51.13	0.98	0.05	0.59	0.02	0.03	0.03	6.58	0.02	0.7	0.6	0.8	0.6	5.40 ± 0.16
Vorab-3	0.20	55.00	0.17	0.04	0.51	0.01	0.03	0.02	1.43	0.01	0.1	0.1	0.5	0.2	2.73 ± 0.10
Vorab-4	0.12	55.37	0.22	0.03	0.45	0.01	0.02	0.03	1.23	0.01	0.2	0.1	0.6	0.2	3.16 ± 0.06
Vorab-5	1.46	51.85	0.51	0.41	0.65	0.01	0.13	0.04	4.76	0.06	0.4	0.3	2.1	0.7	2.81 ± 0.10
Vorab-6	0.13	55.82	0.12	0.02	0.40	0.01	0.02	0.02	0.56	0.00	0.3	0.4	0.4	0.4	0.97 ± 0.03
Vorab-7	0.60	53.30	0.58	0.17	0.53	0.01	0.05	0.06	3.22	0.03	0.4	0.6	0.3	0.8	5.56 ± 0.21
Vorab-8	0.42	54.26	0.57	0.13	0.50	0.01	0.01	0.02	1.85	0.02	0.5	0.5	0.7	0.7	4.10 ± 0.14
Vorab-9	2.01	46.83	1.05	0.55	1.07	0.02	0.14	0.06	11.70	0.11	1.2	0.9	2.3	2.3	8.71 ± 0.15
Vorab-10	1.37	45.39	0.97	0.32	0.98	0.02	0.31	0.04	14.71	0.08	1.1	1	1.7	2	2.99 ± 0.11
Vorab-11	0.23	48.48	0.58	0.02	0.48	0.01	0.01	0.02	9.47	0.01	0.2	0.3	0.7	0.2	3.31 ± 0.05
Vorab-12	0.51	53.64	0.49	0.14	0.55	0.01	0.02	0.03	2.93	0.02	3.5	2.5	1.6	7.4	3.43 ± 0.09
Vorab-13	2.22	40.15	0.92	0.73	1.09	0.02	0.11	0.03	22.70	0.13	1.3	0.9	1.8	2.4	6.12 ± 0.06
Vorab-14	0.34	55.18	0.16	0.10	0.46	0.01	0.01	0.03	0.85	0.02	0.9	0.6	0.6	1.7	2.68 ± 0.03

All bedrock samples located inside the LIA extent, whose true exposure ages should range from about 170 years (just inside of the LIA moraine ridge) to zero years (samples which became ice-free only during the summer of sampling, 2018), have apparent exposure ages that are much too old (3.3–5.8 ka). These samples all contain considerable amounts of ^{36}Cl , which must have been acquired in previous ice-free periods during the Late Glacial and Holocene (shown graphically in Figures 6a and 7). This shows that glacial erosion was not deep enough (>2 m) to remove the cosmogenic signal built up during these ice-free periods [25]. Nevertheless, the apparent exposure ages give evidence of a total minimum exposure they must have experienced, which is an important boundary condition for the numerical modelling.

5.2. MECED Model Results

5.2.1. Evaluation and Definition of Input Parameters

The glacier fluctuation history (periods of coverage of the sampled bedrock by glacier vs. no cover by glacier), the depth of snow and duration of snow cover, as well as the karst

weathering rate applicable to the ice-free periods are the three model input parameters. The most crucial input parameter for the numerical model is the local glacier fluctuation history. A variety of investigative methods have been applied to study and document fluctuations of glaciers in the Alps during the Holocene [46–48]. Local glacier histories have been reconstructed by applying dendrochronological methods and tracking past tree-line variations [49], looking at wood, peat and pollen [50–52] and lake sediment archives [53] and by interpreting historical pictorial data [54] and aerial photographs [55]. Since the 1990s, great inroads have been made into understanding past glacier variations in the Alps through the application of cosmogenic nuclide exposure dating [48,56–61]. This literature and local historic maps were used to construct a glacier fluctuation history for the Vorab glacier (further details given in [25,26]).

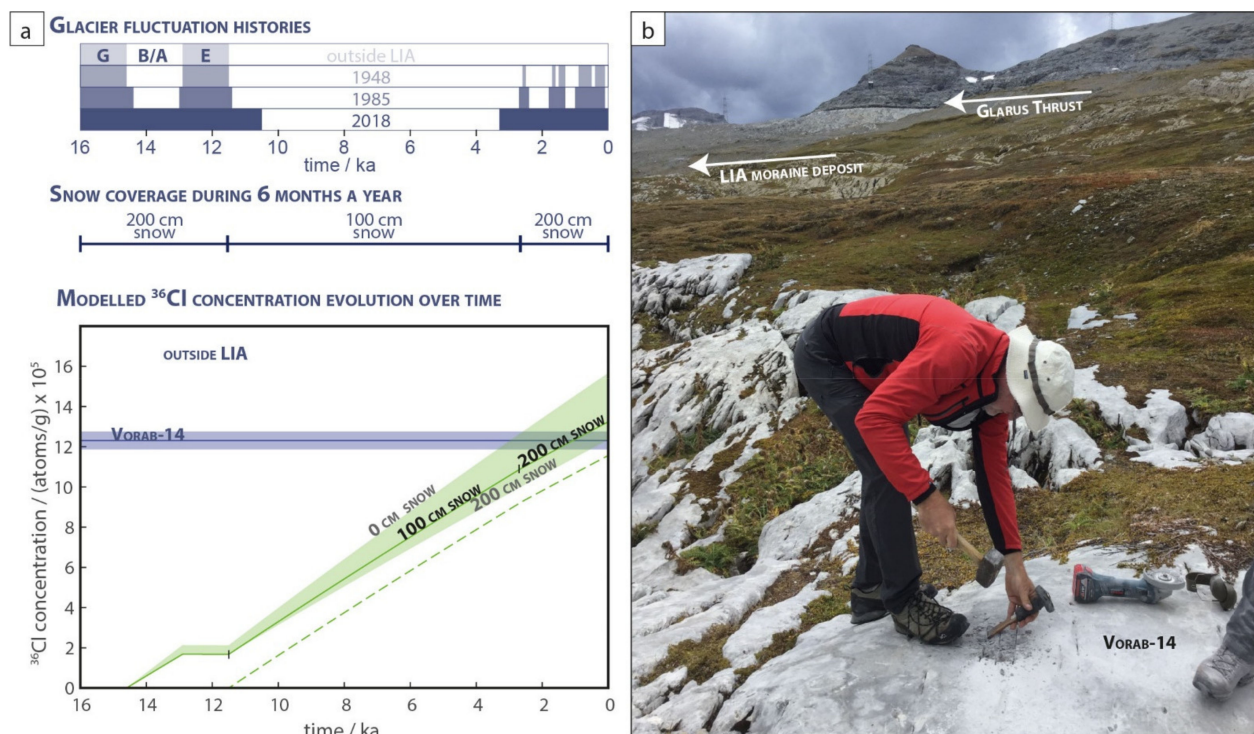


Figure 6. Inputs and output of the MECED model. (a) In the top bar diagram, the blue bars show periods of glacier coverage for each sample group (see Figure 2 and text for details). All sites were covered continuously during the last glacial maximum and Gschnitz stadial glaciers (G) of the Oldest Dryas. All groups except the 2018 group were exposed during the Bølling/Allerød interstadial (B/A) then covered again by the Egesen stadial glacier (E) during the Younger Dryas cold phase. This was followed by a longer ice-free phase before the late Holocene glacier advances. Just below, snow depth input shows that until the end of the Egesen and during the late Holocene 200 cm of snow for 6 months a year was used in the model and only 100 cm of snow during the Holocene warm period in between. The graph below shows the modelled ³⁶Cl concentration increase (solid green line) evolution with time (along the x-axis) for the sample location of Vorab-14 using the glacier fluctuation history for the group outside LIA, showing the increase in ³⁶Cl (green line) during first exposure during the B/A (14.6–12.9 ka), no production while covered by the Egesen stadial glacier (12.9–11.5 ka) and again an increase in ³⁶Cl in the exposed bedrock surface during the entire Holocene. The green band shows the effect of snow depth during ice-free times, where the upper boundary was modelled without any snow and the lower limit by using 200 cm for the entire period. The solid green line used reasonable snow values mentioned in the text. The blue horizontal line shows the AMS-measured ³⁶Cl nuclide concentration along with the uncertainty. The dashed green line shows the modelled concentration if the sample site only became ice-free after the Egesen glacier, highlighting that with this scenario the modelled concentration is lower than the one actually measured, demonstrating why an ice-free period with ³⁶Cl production of the B/A has to be included. (b) Sample location of Vorab-14 with the LIA moraine ridge and the Glarus thrust in the back. See Figures 2 and 3 for the location of samples and photos.

For each sample group (Figure 2) a separate glacier fluctuation history reflecting its location was defined (Figure 6a) based on the literature mentioned above. With these defined glacier histories, the model calculates for every sample the theoretical evolution of the cosmogenic nuclide concentration over time. A representative sample of each group is shown in Figure 7, where the effects of snow and karst weathering rate (see below) are also included. Glacial erosion rates are obtained by dividing the erosion depth by the total time of glacier coverage.

For the samples outside the LIA extent (Vorab-10, Vorab-14) we assume bedrock exposure starting at 14.5 ka with the beginning of the B/A until the Egesen glacier advanced and covered the area again from 12.9 ka to 11.5 ka [48] (Figure 6a). After that, the area outside the LIA was continuously exposed and never covered by a glacier again. The samples of the group 1948 (Vorab-6, Vorab-11, Vorab-12) experienced the same exposure during the B/A and coverage by the Egesen stadial glacier but were additionally repeatedly covered by late Holocene fluctuations of the Vorab glacier from 1.7–1.6 ka, 1.5–1.3 ka, 0.9–0.5 ka and 0.4–0.1 ka (total 2.5 ka of glacier coverage). The samples from the 1985 group (Vorab-7, Vorab-8, Vorab-9) are assumed to have a similar history as the 1950 group but with slightly longer intervals of glacier coverage because they are located at higher elevations and are closer to the present-day glacier front: 13.0–11.4 ka, 2.6–2.4 ka, 1.8–1.3 ka and 1.0–0.1 ka (total 3.3 ka of glacier coverage). It is assumed that the samples from the group 2018 were ice-covered until the early Holocene, when the Egesen stadial glacier retreated around 10.5 ka ago. During the late Holocene, it is likely that these areas were continuously glacier-covered from 3.3 ka until the summer of sampling (2018).

Snow depth data were derived by looking at records from the nearest station. According to the MeteoSchweiz [Schweizerische Eidgenossenschaft 2019] data, the station at Crap Masegn (Figure 1) (2480 m a.s.l.) is the nearest station. Precipitation records there span the past 30 years. The data show that at this elevation a constant snow cover of about 200 cm can be assumed for 6 months of the year. Knowing that during the middle Holocene warm phase [50,62] it is likely that there was less snow, we assume for this time period a reduced snow cover of 100 cm for 6 months a year. As shown in Figure 6, for our model we use 200 cm snow before the Holocene, 100 cm snow during the early and middle Holocene and 200 cm snow after 3.6 ka.

However, we are aware that these values are estimates. To visualise the effect of different snow depth values on the modelled ^{36}Cl concentration, minimal and maximal snow scenarios are indicated in Figures 6b and 7 as green bands. The upper limit of the green band tracks the modelled growth of ^{36}Cl in the bedrock with no snow cover at all and the lower limit of the green band tracks the modelled growth when a depth of 200 cm of snow is considered for all ice-free periods (including during the middle Holocene). The influence on the final modelled ^{36}Cl concentration in comparison to our chosen input parameters is about +15% (no snow) and -10% (200 cm of snow all of the time the forefield is ice-free). If the snow depth were further increased (>200 cm), for many locations it would not be possible to calculate erosion depth/rate values, as the modelled nuclide concentration would get lower than the actual AMS-measured one. The karst weathering rate of 5 mm ka^{-1} , a reasonable value for limestone surfaces in the Alps [63–65] causes a reduction on the modelled concentration of about 5%.

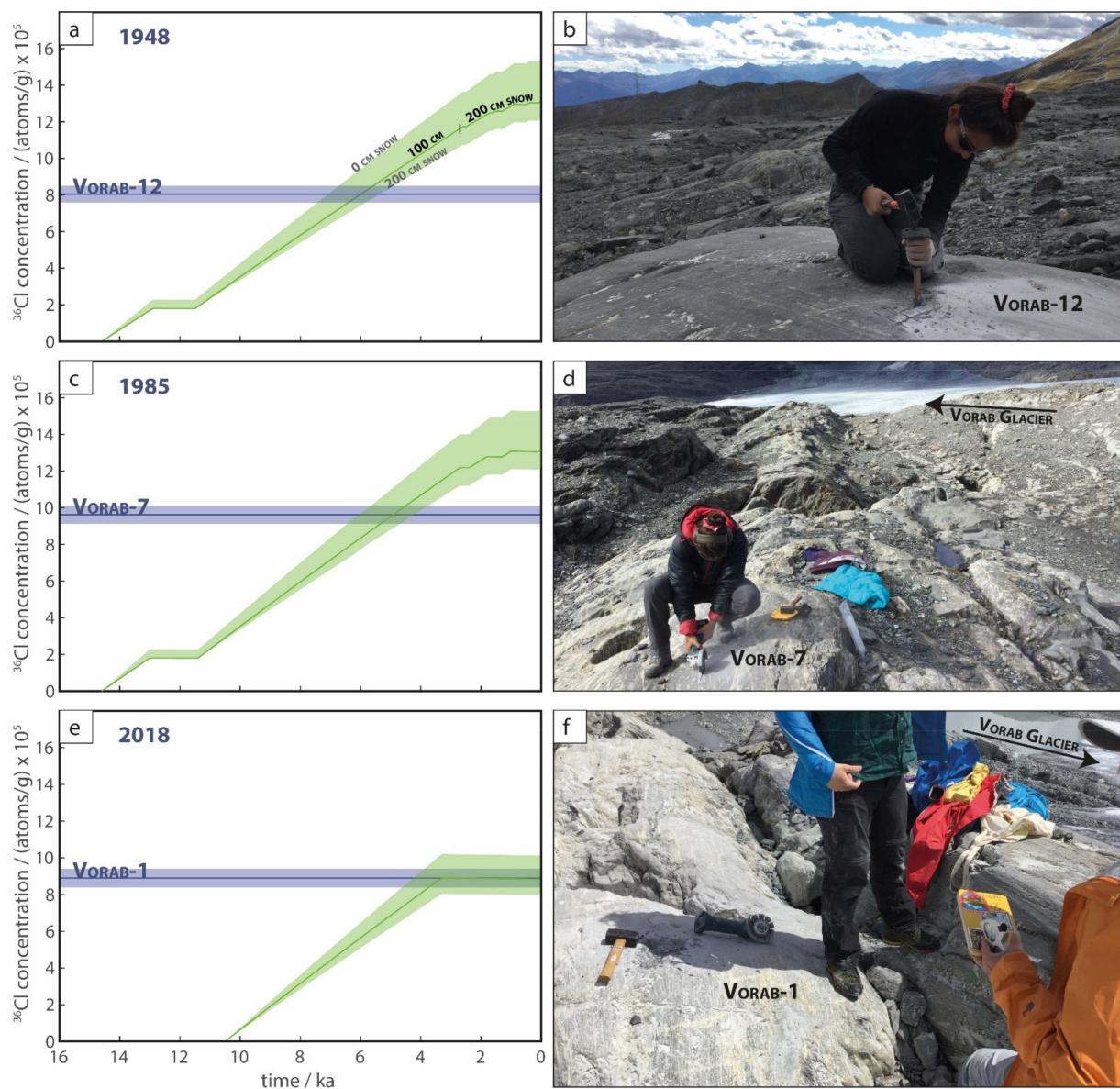


Figure 7. (a,c,e) MECED model output for a representative sample (Vorab-12, Vorab-7, Vorab1) of each group (1948, 1985, 2018) inside the LIA extent, showing the increase in ^{36}Cl during ice-free periods and no production during phases of glacier coverage (stays flat). (b,d,f) shows a photo of the corresponding sample. For a detailed description of the diagrams see caption of Figure 6. See Figures 2 and 3 for the location of samples and photos.

5.2.2. Glacial Erosion Depths and Rates

For every sample individually, the modelled depth profile of the nuclide concentration, including all the appropriate parameters described before, and the AMS measured ^{36}Cl concentrations were used to calculate the subglacial erosion depth [25] (Figure 8). Divided by the duration of the glacier cover we then obtained the average erosion rate values. An overview on the calculated erosion depths and erosion rates for all samples (excluding data from boulder Vorab-13) is given in Table 3 and Figure 9. Determined glacial erosion depths for the 2018 sample group are between 0 cm and 40 cm, with corresponding erosion rates of 0–0.12 mm a^{-1} . Erosion depth values for the group 1985 range from 17.8 cm to 52.7 cm resulting in erosion rates of 0.05–0.16 mm a^{-1} . For the group near the LIA extent (1948) erosion depths of 11.8–35.9 cm and erosion rates from 0.05–0.14 mm a^{-1} were determined. For outside the LIA extent, an erosion depth of 2.5–2.7 cm and an erosion rate of 0.02–0.05 mm a^{-1} could be calculated only for Vorab-14. The measured ^{36}Cl

concentration of Vorab-10 was higher than the modelled one and thus it was not possible to determine erosion depth or rate. This means the data from this location, especially the measured ^{36}Cl concentration, do not allow the calculation of rock depth removed or glacial erosion rates. This would only be possible if the time of ice-free phases were increased. However, this seems rather unrealistic due to relatively high elevation of the location (2439 m a.s.l.) and considering that during the Younger Dryas the Vorab glacier reached several km further down-valley than its LIA position [66–68].

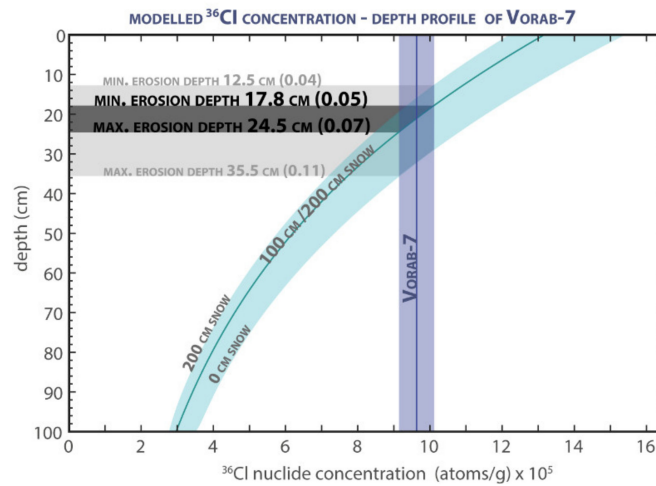


Figure 8. Modelled ^{36}Cl concentration-depth profile (light-blue) using the elemental and location data of Vorab-7. The solid line used the 200–100–200 cm snow scenario (see Figure 6 for details), the light blue band indicates the two extreme snow scenarios (0 cm snow and 200 cm snow). The AMS-measured concentration with its uncertainty is shown as vertical line in dark blue. The intersection of the two curves indicates the thickness of rock that had to be removed by the glacier to reach measured concentration (Table 1). The dark grey band highlights the erosion depth range (Table 3) with the intermediate snow scenario, the light grey indicates the minimal erosion depth when considering the 200 cm snow scenario and the maximal erosion depth with the zero snow scenario. By dividing this erosion depth by the total time of glacier coverage results in the average glacial erosion rates, given in parentheses.

Table 3. Determined glacial erosion depths and rates (sample locations in Figure 9).

Sample	Erosion Depth cm	Erosion Rate mm a^{-1}
Glacier front 2018		
Vorab-1	0.0–3.5	0.00–0.01
Vorab-2	0.0–4.1	0.00–0.01
Vorab-3	0.0–2.5	0.00–0.01
Vorab-4	3.1–8.8	0.01–0.03
Vorab-5	32.2–39.5	0.10–0.12
Glacier front 1985		
Vorab-7	17.8–24.5	0.05–0.07
Vorab-8	30.4–38.7	0.09–0.12
Vorab-9	46.0–53.7	0.14–0.16
Glacier front 1948		
Vorab-6	11.8–18.9	0.05–0.08
Vorab-11	24.3–32.6	0.10–0.13
Vorab-12	28.5–35.9	0.11–0.14
Outside LIA extent		
Vorab-10	nv–nv	nv–nv
Vorab-14	2.5–7.2	0.02–0.05

nv: no value.

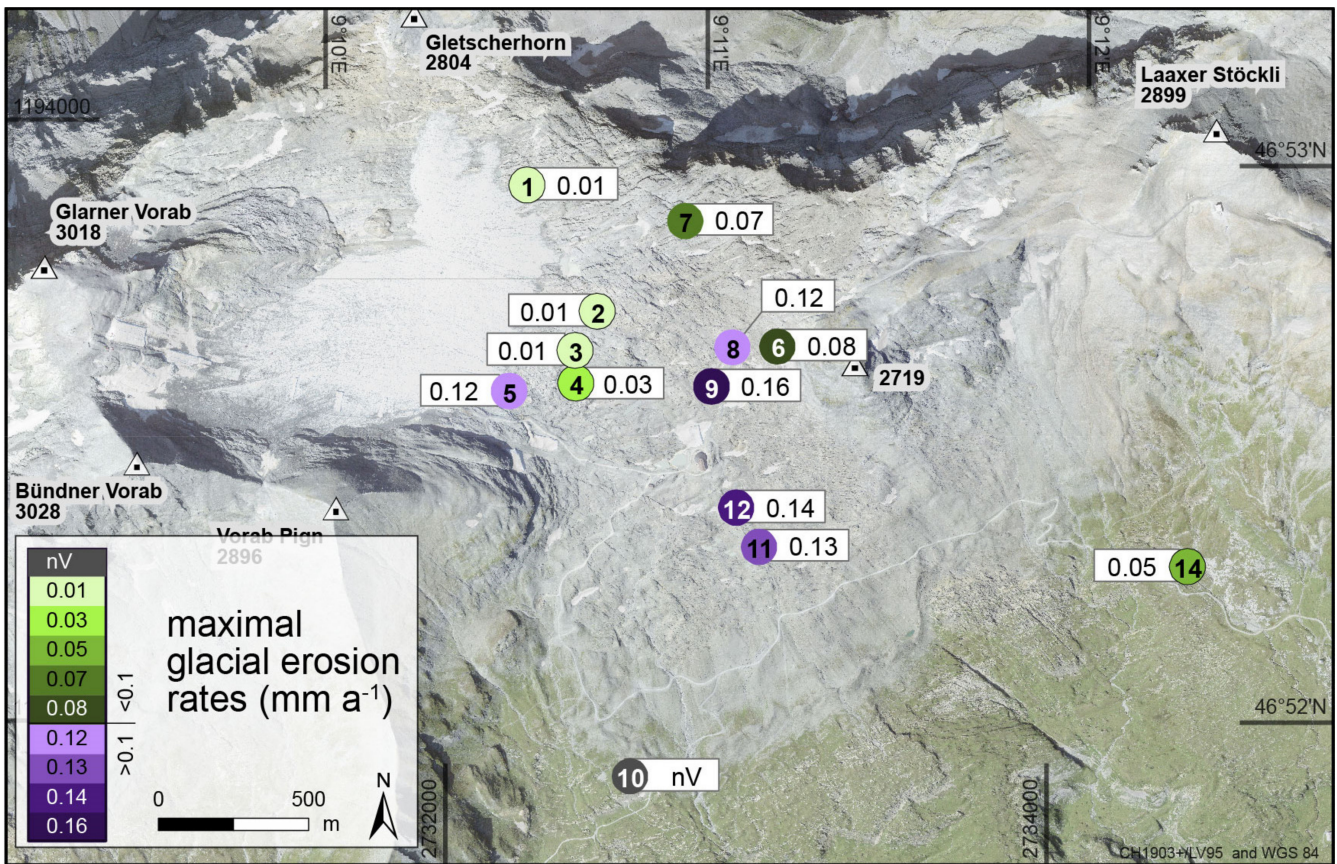


Figure 9. Determined maximal glacial erosion rates given in mm a^{-1} (Table 3). Green colours indicate glacial erosion rates less than and violet colours more than 0.1 mm a^{-1} . 3D view created with the swissIMAGE orthophoto 2019 and the SwissALTI3D 2019 (reproduced with authorization of the Swiss Federal Office of Topography, swisstopo).

6. Discussion and Conclusions

It is beyond question that the present-day shape of the Alps is the result of glacial erosion over numerous episodes of an extensive ice cap nearly completely covering the mountains and reaching to the forelands. However, actually determining glacial erosion rates remains challenging because conducting direct measurements is still extremely difficult [14]. Using cosmogenic nuclides in combination with a numerical model has been shown to be a strong tool for obtaining local glacial erosion rate values directly determined on glacially abraded bedrock surfaces [25,26]. As in the present investigation at the Vorab glacier, these studies give insight not only on local glacial and landscape forming processes but also increase understanding of the formation and evolution of the overall Alpine landscape.

At Vorab, the obtained high ^{36}Cl concentrations and calculated apparent exposure ages inside of the LIA extent between 7.1 ka to 3.3 ka provide clear evidence of the very small amount of erosion ($<2 \text{ m}$ deep) accomplished by the glacier during the late Holocene. The bedrock surfaces sampled were covered during the LIA as shown by historical maps (Figure 2). Coverage during the frequent cold phases of the late Holocene can be inferred from the numerous Holocene glacier variation studies carried out in the Alps (see Section 5.2.2). Accordingly, determined glacial erosion rates in the entire study area are low; all are less than $<0.23 \text{ mm a}^{-1}$. We recognize a faint spatial pattern in the measured erosion rates across the glacier forefield as indicated by the colour coding in Figure 9. Erosion rates are lowest near the present-day glacier front (Vorab-1, Vorab-2, Vorab-3, Vorab-4, Vorab-5; green in Figure 9) and highest in the central part of the glacier forefield (Vorab-8: 0.12 mm a^{-1} , Vorab-9: 0.16 mm a^{-1} ; purple in Figure 9). Vorab-6 is

relatively close to these high values, with a rate of 0.08 mm a^{-1} . This slight local decrease in erosion efficiency could be due to its position. Vorab-6 is located where the slope slowly increases towards the approximately 100 m high bedrock ridge between Laaxer Stöckli and peak 2719. Here, the glacier flowed predominantly either to the left (northeast) or to the right (southward) as the bedrock ridge blocked its progress (see Figure 2). Our data also point to a slight increase in glacial erosion rate from north (Vorab-1: 0.01 mm a^{-1} and Vorab-7: 0.07 mm a^{-1}) to south (Vorab-5: 0.12 mm a^{-1} and Vorab-9: 0.23 mm a^{-1}). The glacial erosion rate determined from a bedrock sample outside of the LIA ice margin (Vorab-14) indicates that even during the Younger Dryas, during the Egesen stadial, the Vorab glacier was eroding at a very low rate of only 0.05 mm a^{-1} . However, it is important to keep the uncertainties of the input parameters of the MECED model in mind. Small changes in the glacier fluctuation history and the snow depth would slightly shift the erosion rate values. Nevertheless, because the input parameters were chosen conservatively to allow maximal erosion values within reasonable boundaries, the values should stay low or indeed get even lower. A thorough discussion of the effects of the input parameters is found in [25].

Our determined low glacial erosion rates are supported by field observations. On first sight, the forefield of the Vorab glacier appears to be strongly abraded by the glacier, as indicated by the heavily striated and highly polished bedrock surfaces. Taking a closer look, this only seems true for the previously present (i.e., before they were eroded) Verrucano and schistose lithologies that overlie the limestone. A crucial point is that in general, there is very little glacial sediment in the entire glacier forefield; most is bare limestone. Clasts are almost exclusively comprised Permian Verrucano, whereas limestone clasts are extremely rare and only found in the northern part of the study area. The same is true for the stone stripes, suggesting that the origin of these stone stripes is Permian bedrock obstacles below the glacier. In light of this isotopic and field evidence, we suggest that over many glacier advances, the glacier planed off the rock above the Glarus thrust (Permian Verrucano). As soon as the glacier eroded down to the Glarus thrust, where the lithology changes to limestone, its ability to erode dropped off decidedly. The Glarus thrust and the (remaining) overlying Verrucano units outcrop on both sides of the gap between Vorab Pign and peak 2719 (Figure 2). The glacier must have constantly widened instead of deepened this gap to head southward. In the passage through this gap and to the south, there are no remnants of Permian rock in the glacier forefield. The bedrock steps there indicate that plucking, not abrasion, is likely the dominant erosion process in the limestone units.

Field observations (numerous swallow holes and channels) are evidence that the limestone forefield is strongly karstified. Meltwater drains into a subsurface karst network to emanate in springs like those near Flims and Laax (Figure 1) [44,69]. The rapid loss of subglacial water into the karst system is likely the main factor for the low glacial erosion [25]. As a consequence of the lacking subglacial meltwater, the sliding capability of the glacier is reduced which directly influences the ability of the glacier to erode (abrade) the underlying bedrock [9,18,20,70,71]. This inhibition of sliding and low rate of erosion leads to low rates of subglacial sediment production. As noted above, there is almost no fine subglacial sediment in the glacier forefield. The limestones are massive and thick-bedded making them less susceptible to glacial erosion. This likely played a part in allowing the limestone plateau to develop as the Vorab glacier methodically shaved off the bedrock above the Glarus thrust (cf. [25]).

In this study, several factors were observed which are responsible for the formation of the limestone plateau in front of the Vorab glacier. These include the presence of: (i) the sharp geological contact (Glarus thrust), (ii) the massive, thick-bedded limestone below the thrust plane and (iii) the presence of a well-developed karst system. Similar findings were reported from the Lapis de Tsanfleuron (Figure 1) [25] and strengthen the hypothesis that high-elevation, low-relief limestone plateaus form due to limited glacial erosion because the glacier has a significantly reduced ability to slide as a consequence of losing water at the glacier bed into a well-developed karst system. At the Lapis de Tsanfleuron, an even more extensive limestone plateau, determined glacial erosion rate values were similarly

low or even lower ($<0.08 \text{ mm a}^{-1}$) than those we determined at the Vorab glacier. The main difference between the two sites is the presence of the Glarus thrust plane right at the flat Vorab glacier forefield. Elevation (2600 m a.s.l.), aspect (east-facing) and precipitation values (150–200 m of snow) are comparable at both sites. Other striking similarities of the two sites are the absence of abundant glacial sediment, the presence of sediment stripes in glacier flow direction and the bedrock steps. Such clean (sediment-free) limestone plateaus at high elevations with associated underlying karst are common landscapes in the Alps, e.g., Hallstätter glacier, Dachstein Massif, Steinernes Meer, Siebenhengste and Hölloch-Silberen.

Glacial erosion rates determined on limestone beds are one to two orders of magnitude lower than those determined at sites located on crystalline bedrock, e.g., Rhône glacier (up to 0.66 mm a^{-1}) [24], Trift glacier ($>1.8 \text{ mm a}^{-1}$) [26] (locations in Figure 1). In both of these crystalline study sites, the authors found a clear trend of low erosion rates at the margin of the glacier, where rates become nearly zero, while the highest erosion rates are measured below the central flow line of the glacier. At Trift glacier, rates of several millimetres per year were calculated from sites at the centre of the overdeepened glacial valley. In contrast, at the Lapis de Tsanfleuron and at the Vorab glacier, no significant or similarly extreme spatial variations in erosion rates were observed. Intriguingly, the slight decrease in glacial erosion that we noted at Vorab (Figure 9) occurs along the central flowline, the direct opposite of what was observed at Trift and the Rhône glacier. These stark differences in glacial erosion rates reveal quantitatively how the respective glaciers are carving quite distinct topographies. Whereas in limestone-dominated areas glacier forefields are plateau-shaped (broad and flat with very little relief); in crystalline areas (granite/gneiss) deep steep-walled valleys and at many sites overdeepened basins, e.g., the Rhône glacier and Trift glacier (Figure 1), tend to develop. The formation of overdeepenings is complex and usually a combination of geological (fracture spacing, weak zones, change in lithology) [72–74], geographical (glacier confluences) [75,76] and glaciological (near equilibrium line altitude, rates of ice flux) [12,77–79] factors. Recent research at Trift glacier, where there is an exceptionally deep overdeepening, highlighted that the presence of a gorge seems to have a crucial effect on the formation and the apparent depth of an overdeepening [26].

Undoubtedly many factors like elevation, precipitation sums, aspect, slope and bedrock geology influence the glacier and its behaviour, making the situation very complex and general statements on glacial erosion rates difficult. Nevertheless, recent studies on glacial erosion efficiency [24–26,80] highlight that there seems to be a relatively simple correlation between lithology, hydrology and glacial erosion rates. In crystalline areas (compact, impermeable bedrock) with an intact subglacial hydrology (subglacial meltwater present), glaciers tend to erode the bedrock strongly along the central flowline but only slightly near the lateral ice margins. Over hundreds of thousands of years this leads to the development of long, narrow, often overdeepened, steep-walled valleys. In contrast, flat glacier forefields form in areas dominated by horizontally bedded massive limestone with a well-developed karst system. Through the effective drainage of subglacial meltwater into the karst system, the ability of the glacier to slide is sharply curtailed. This results in an inability to erode the underlying substrate, favouring the formation of broad and flat landscapes (plateaus). A positive feedback loop develops: the glacier planes off a flat plateau as it reaches the massive flat-bedded limestone; the gentler the slope the further that sliding is inhibited. Over time, as these flat landscape elements cannot be reduced by glaciers, they evolve into plateaus—high-elevation islands. Despite the interplay of numerous factors, the importance of glaciers in the construction of mountainous landscapes is due as much to their ability to erode as to their ability to not erode.

Author Contributions: Conceptualization of the study was done by S.I.-O. and O.S.; methodology by A.M., O.S. and C.V.; investigation by A.M., S.I.-O., V.P. and O.S.; formal analysis by A.M. and O.S.; data curation by C.V., A.M. and O.S.; writing—original draft preparation, O.S., S.I.-O. and A.M.; writing—review and editing O.S. and S.I.-O.; visualisation, O.S. and A.M.; supervision, S.I.-O. and

V.P.; funding acquisition by S.I.-O. All authors have read and agreed to the published version of the manuscript.

Funding: Funding for this project was provided by “Schweizerischer Nationalfonds zur Förderung der Wissenschaftlichen Forschung” (SNSF) Project 175794 and 156187.

Data Availability Statement: All data are published within the publication.

Acknowledgments: We thank Sarah Kamleitner, Basil Weber and Ueli Steinemann for their support during fieldwork and Stefano Casale for his assistance in the laboratory. We are grateful for the overall support of the Laboratory of Ion Beam physics group and their excellent AMS measurements. Special thanks to the community of Laax and to the Weisse Arena Gruppe for providing driving permission and suitable vehicles for comfortable access to the study area. Funding for this project was provided by “Schweizerischer Nationalfonds zur Förderung der Wissenschaftlichen Forschung” (SNSF) Project 175794 and 156187. MeteoSchweiz (the Swiss Federal Office of Meteorology and Climatology) and Swisstopo (Federal Office of Topography swisstopo, provided local weather and geo data.

Conflicts of Interest: The authors declare no conflict of interest. The funders had no role in the design of the study; in the collection, analyses or interpretation of data; in the writing of the manuscript, or in the decision to publish the results.

References

1. Penck, A.; Brückner, E. *Die Alpen im Eiszeitalter*; Tauchitz: Leipzig, Germany, 1909.
2. Wright, G.F. The Muir Glacier. *Sci. Am.* **1887**, *23*, 9252. [[CrossRef](#)]
3. Agassiz, L. On the polished and striated surfaces of the rocks which form the beds of glaciers in the Alps. In *Proceedings of the Geological Society London*; Geological Society of London: London, UK, 1838; Volume 3, pp. 321–322.
4. Davis, W.M. The sculpture of mountains by glaciers. *Scott. Geogr. Mag.* **1906**, *22*, 76–89. [[CrossRef](#)]
5. Jordan, P. Analysis of overdeepened valleys using the digital elevation model of the bedrock surface of Northern Switzerland. *Swiss J. Geosci.* **2010**, *103*, 375–384. [[CrossRef](#)]
6. Preusser, F.; Reitner, J.; Schlüchter, C. Distribution, geometry, age and origin of overdeepened valleys and basins in the Alps and their foreland. *Swiss J. Geosci.* **2010**, *103*, 407–426. [[CrossRef](#)]
7. Dürst Stucki, M.; Schlunegger, F. Identification of erosional mechanisms during past glaciations based on a bedrock surface model of the central European Alps. *Earth Planet. Sci. Lett.* **2013**, *384*, 57–70. [[CrossRef](#)]
8. Sternai, P.; Herman, F.; Champagnac, J.-D.; Fox, M.; Salcher, B.; Willett, S.D. Pre-glacial topography of the European Alps. *Geology* **2012**, *40*, 1067–1070. [[CrossRef](#)]
9. Herman, F.; Beaud, F.; Champagnac, J.D.; Lemieux, J.M.; Sternai, P. Glacial hydrology and erosion patterns: A mechanism for carving glacial valleys. *Earth Planet. Sci. Lett.* **2011**, *310*, 498–508. [[CrossRef](#)]
10. Hinderer, M.; Kastowski, M.; Kamelger, A.; Bartolini, C.; Schlunegger, F. River loads and modern denudation of the Alps—A review. *Earth-Sci. Rev.* **2012**, *118*, 11–44. [[CrossRef](#)]
11. Herman, F.; De Doncker, F.; Delaney, I.; Prasicek, G.; Koppes, M. The impact of glaciers on mountain erosion. *Nat. Rev. Earth Environ.* **2021**. [[CrossRef](#)]
12. Cook, S.J.; Swift, D.A. Subglacial basins: Their origin and importance in glacial systems and landscapes. *Earth-Sci. Rev.* **2012**, *115*, 332–372. [[CrossRef](#)]
13. Boulton, G.S. Processes and Patterns of Glacial Erosion. In *Glacial Geomorphology*; Coates, D.R., Ed.; Springer: Dordrecht, The Netherlands, 1982; pp. 41–87. [[CrossRef](#)]
14. Lütsch-Loetscher, O. 4. Kapitel. Die Bedeutung und Bewertung der Vorratsänderungen im Wasserhaushalt der Gletscher im Schweizer Hochgebirge, 5. Kapitel. Beobachtungen über das Verhalten des vorstossenden Obern Grindelwaldgletschers im Berner Oberland. In *Zum Wasserhaushalt Des Schweizer Hochgebirgers*; Kümmerly & Frey: Bern, Switzerland, 1944.
15. Bezinge, A.; Clark, M.J.; Gurnell, A.M.; Warburton, J. The management of sediment transported by glacial melt-water streams and its significance for the estimation of sediment yield. *Ann. Glaciol.* **1989**, *13*, 1–5. [[CrossRef](#)]
16. Bogen, J. Erosion rates and sediment yields of glaciers. *Ann. Glaciol.* **1996**, *22*, 48–52. [[CrossRef](#)]
17. Beaud, F.; Flowers, G.E.; Venditti, J.G. Efficacy of bedrock erosion by subglacial water flow. *Earth Surf. Dyn.* **2016**, *4*, 125–145. [[CrossRef](#)]
18. Cook, S.J.; Swift, D.A.; Kirkbride, M.P.; Knight, P.G.; Waller, R.I. The empirical basis for modelling glacial erosion rates. *Nat. Commun.* **2020**, *11*, 1–7. [[CrossRef](#)]
19. MacGregor, K.R.; Anderson, R.S.; Waddington, E.D. Numerical modeling of glacial erosion and headwall processes in alpine valleys. *Geomorphology* **2009**, *103*, 189–204. [[CrossRef](#)]
20. Koppes, M.; Hallet, B.; Rignot, E.; Mouginot, J.; Wellner, J.S.; Boldt, K. Observed latitudinal variations in erosion as a function of glacier dynamics. *Nature* **2015**, *526*, 100. [[CrossRef](#)]

21. Cohen, D.; Gillet-Chaulet, F.; Haeblerli, W.; Machguth, H.; Fischer, U.H. Numerical reconstructions of the flow and basal conditions of the Rhine glacier, European Central Alps, at the Last Glacial Maximum. *Cryosphere* **2018**, *12*, 2515–2544. [[CrossRef](#)]
22. Seguinot, J.; Delaney, I. Last glacial cycle glacier erosion potential in the Alps. *Earth Surf. Dyn. Discuss.* **2021**, *9*, 923–935. [[CrossRef](#)]
23. Wirsig, C.; Ivy-Ochs, S.; Reitner, J.M.; Christl, M.; Vockenhuber, C.; Bichler, M.; Reindl, M. Subglacial abrasion rates at Goldbergkees, Hohe Tauern, Austria, determined from cosmogenic ^{10}Be and ^{36}Cl concentrations. *Earth Surf. Process. Landf.* **2017**, *42*, 1119–1131. [[CrossRef](#)]
24. Goehring, B.M.; Schaefer, J.M.; Schlüchter, C.; Lifton, N.A.; Finkel, R.C.; Jull, A.T.; Akçar, N.; Alley, R.B. The Rhone Glacier was smaller than today for most of the Holocene. *Geology* **2011**, *39*, 679–682. [[CrossRef](#)]
25. Steinemann, O.; Ivy-Ochs, S.; Grazioli, S.; Luetscher, M.; Fischer, U.H.; Vockenhuber, C.; Synal, H.A. Quantifying glacial erosion on a limestone bed and the relevance for landscape development in the Alps. *Earth Surf. Process. Landf.* **2020**, *45*, 1401–1417. [[CrossRef](#)]
26. Steinemann, O.; Ivy-Ochs, S.; Hippe, K.; Christl, M.; Haghipour, N.; Synal, H.A. Glacial erosion by the Trift glacier (Switzerland): Deciphering the development of riegels, rock basins and gorges. *Geomorphology* **2021**, *375*, 107533. [[CrossRef](#)]
27. GLAMOS The Swiss glaciers 1880-2016/17, Glaciological reports No 1-138. In *Yearbooks of the Cryospheric Commission of the Swiss Academy of Sciences (SCNAT) 1881–2019*; Published since 1964; VAW/ETH: Zürich, Switzerland; Available online: <https://www.glamos.ch> (accessed on 30 June 2021). [[CrossRef](#)]
28. Garwood, E.J. Features of Alpine Scenery Due to Glacial Protection. *Geogr. J.* **1910**, *36*, 310–336. [[CrossRef](#)]
29. Buckingham, T.; Pfiffner, O.A. Mountain Building and Valley Formation in the UNESCO World Heritage Tectonic Arena Sardona Region. In *Landscapes and Landforms of Switzerland*; Reynard, E., Ed.; Springer: Cham, Switzerland, 2021; pp. 173–186. [[CrossRef](#)]
30. Pfiffner, O.A. Structural map of the Helvetic Zone of the Swiss Alps: Including Vorarlberg (Austria) and Haute Savoie (France). *Geological Special Map 128/1-7* **2010**.
31. Pfiffner, O.A. Tektonische Untersuchungen im Infrahelvetikum der Ostschweiz. Ph.D. Thesis, ETH Zürich und Universität Zürich, Zürich, Switzerland, 1977.
32. Ivy-Ochs, S.; Synal, H.A.; Roth, C.; Schaller, M. Initial results from isotope dilution for Cl and ^{36}Cl measurements at the PSI/ETH Zurich AMS facility. *Nucl. Instrum. Methods Phys. Res. Sect B Beam Interact. Mater. At.* **2004**, *223*, 623–627. [[CrossRef](#)]
33. Stone, J.O.; Allan, G.L.; Fifield, L.K.; Cresswell, R.G. Cosmogenic chlorine-36 from calcium spallation. *Geochim. Cosmochim. Acta* **1996**, *60*, 679–692. [[CrossRef](#)]
34. Vockenhuber, C.; Miltenberger, K.U.; Synal, H.A. ^{36}Cl measurements with a gas-filled magnet at 6 MV. *Nucl. Instrum. Methods Phys. Res. Sect B Beam Interact. Mater. At.* **2019**, *455*, 190–194. [[CrossRef](#)]
35. Alfimov, V.; Ivy-Ochs, S. How well do we understand production of ^{36}Cl in limestone and dolomite? *Quat. Geochronol.* **2009**, *4*, 462–474. [[CrossRef](#)]
36. Steinemann, O. Using cosmogenic nuclides to understand rockglacier dynamics during the Lateglacial and to quantify glacial erosion on limestone and gneiss in the Alps. Ph.D. Thesis, ETH Zürich, Zürich, Switzerland, 2020.
37. Wirsig, C. Constraining the Timing of Deglaciation of the High Alps and Rates of Subglacial Erosion with Cosmogenic Nuclides. Ph.D. Thesis, ETH Zürich, Zürich, Switzerland, 2015.
38. Dufour, G.H.; Müllhaupt, H.; Stempelmann, J.; Kögel, H. *Altdorf, Chur*; Eidg. Topographisches Bureau: Genf, Switzerland, 1859.
39. Online Karten viewer. Available online: www.maps.geo.admin.ch (accessed on 6 June 2021).
40. Lukas, S.; Rother, H. Moränen versus Till: Empfehlungen für die Beschreibung, Interpretation und Klassifikation glazialer Landformen und Sedimente. *E&G Quat. Sci. J.* **2016**, *65*, 95–112. [[CrossRef](#)]
41. Keller, B. Lithofazies-Codes für die Klassifikation von Lockergesteinen. *Mitteilungen Schweiz. Ges. Boden- u. Felsmechanik* **1996**, *132*, 5–12.
42. Bögli, A. *Karst Hydrology and Physical Speleology*; Springer: Berlin, Germany, 1980. [[CrossRef](#)]
43. Veress, M.; Telbisz, T.; Tóth, G.; Lóczy, D.; Ruban, D.A.; Gutak, J.M. *Glaciokarsts*; Springer: Cham, Switzerland, 2019. [[CrossRef](#)]
44. Häuselmann, P.; Jeannin, P.Y. Wasserwege der Gemeinde Flims und ihre Einflüsse auf den Caumasee. *Schweiz. Inst. Speläologie und Karstforschung* **2009**, *24*, 1–24.
45. Christl, M.; Vockenhuber, C.; Kubik, P.W.; Wacker, L.; Lachner, J.; Alfimov, V.; Synal, H.A. The ETH Zurich AMS facilities: Performance parameters and reference materials. *Nucl. Instrum. Methods Phys. Res. Sect B Beam Interact. Mater. At.* **2013**, *294*, 29–38. [[CrossRef](#)]
46. Schneebeil, W.; Röthlisberger, F. 8000 Jahre Walliser Gletschergeschichte ein Beitrag zur Erforschung des Klimaverlaufs in der Nacheiszeit. Ph.D. Dissertation, University of Zürich, Verlag Schweizer Alpen-Club, Bern, Switzerland, 1976.
47. Holzhauser, H. Gletscherschwankungen innerhalb der letzten 3200 Jahre am Beispiel des grossen Aletsch- und des Gornergletschers. Neue Ergebnisse. In *Gletscher im Ständigen Wandel*; vdf Hochschulverlag AG an der ETH Zürich: Zürich, Switzerland, 1995; pp. 101–123.
48. Ivy-Ochs, S.; Kerschner, H.; Maisch, M.; Christl, M.; Kubik, P.W.; Schlüchter, C. Latest Pleistocene and Holocene glacier variations in the European Alps. *Quat. Sci. Rev.* **2009**, *28*, 2137–2149. [[CrossRef](#)]
49. Holzhauser, H. *Auf dem Holzweg zur Gletschergeschichte*; Mitteilungen Naturforschende Gesellschaft in Bern: Bern, Switzerland, 2009; Volume 66, pp. 173–208.

50. Hormes, A.; Müller, B.U.; Schlüchter, C. The Alps with little ice: Evidence for eight Holocene phases of reduced glacier extent in the Central Swiss Alps. *Holocene* **2001**, *11*, 255–265. [[CrossRef](#)]
51. Joerin, U.E.; Stocker, T.F.; Schlüchter, C. Multicentury glacier fluctuations in the Swiss Alps during the Holocene. *Holocene* **2006**, *16*, 697–704. [[CrossRef](#)]
52. Wick, L. Vegetational response to climatic changes recorded in Swiss Late Glacial lake sediments. *Palaeogeogr. Palaeoclimatol. Palaeoecol.* **2000**, *159*, 231–250. [[CrossRef](#)]
53. Leemann, A.; Niessen, F. Holocene glacial activity and climatic variations in the Swiss Alps: Reconstructing a continuous record from proglacial lake sediments. *Holocene* **1994**, *4*, 259–268. [[CrossRef](#)]
54. Zumbühl, H.J.; Nussbaumer, S.U. Little Ice Age glacier history of the Central and Western Alps from pictorial documents. *Cuad. Investig. Geogr.* **2018**, *44*, 115–136. [[CrossRef](#)]
55. Bauder, A.; Funk, M.; Huss, M. Ice-volume changes of selected glaciers in the Swiss Alps since the end of the 19th century. *Ann. Glaciol.* **2007**, *46*. [[CrossRef](#)]
56. Le Roy, M.; Deline, P.; Carcaillet, J.; Schimmelpfennig, I.; Ermini, M. ¹⁰Be exposure dating of the timing of Neoglacial glacier advances in the Ecrins-Pelvoux massif, southern French Alps. *Quat. Sci. Rev.* **2017**, *178*, 118–138. [[CrossRef](#)]
57. Le Roy, M.; Nicolussi, K.; Deline, P.; Astrade, L.; Edouard, J.L.; Miramont, C.; Arnaud, F. Calendar-dated glacier variations in the western European Alps during the Neoglacial: The Mer de Glace record, Mont Blanc massif. *Quat. Sci. Rev.* **2015**, *108*, 1–22. [[CrossRef](#)]
58. Schimmelpfennig, I.; Schaefer, J.M.; Akçar, N.; Ivy-Ochs, S.; Finkel, R.C.; Schlüchter, C. Holocene glacier culminations in the Western Alps and their hemispheric relevance. *Geology* **2012**, *40*, 891–894. [[CrossRef](#)]
59. Schimmelpfennig, I.; Schaefer, J.M.; Akçar, N.; Koffman, T.; Ivy-Ochs, S.; Schwartz, R.; Finkel, R.C.; Zimmerman, S.; Schlüchter, C. A chronology of Holocene and Little Ice Age glacier culminations of the Steingletscher, Central Alps, Switzerland, based on high-sensitivity beryllium-10 moraine dating. *Earth Planet. Sci. Lett.* **2014**, *393*, 220–230. [[CrossRef](#)]
60. Kronig, O.; Ivy-Ochs, S.; Hajdas, I.; Christl, M.; Wirsig, C.; Schlüchter, C. Holocene evolution of the Triftjè- and the Oberseegletscher (Swiss Alps) constrained with ¹⁰Be exposure and radiocarbon dating. *Swiss J. Geosci.* **2018**, *111*, 117–131. [[CrossRef](#)]
61. Protin, M.; Schimmelpfennig, I.; Mugnier, J.-L.; Buoncristiani, J.-F.; Le Roy, M.; Pohl, B.; Moreau, L.; ASTER Team; Aumaître, G.; Boulès, D.; et al. Millennial-scale deglaciation across the European Alps at the transition between the Younger Dryas and the Early Holocene—Evidence from a new cosmogenic nuclide chronology. *Boreas* **2021**, *50*, 671–685. [[CrossRef](#)]
62. Joerin, U.E.; Nicolussi, K.; Fischer, A.; Stocker, T.F.; Schlüchter, C. Holocene optimum events inferred from subglacial sediments at Tschierva Glacier, Eastern Swiss Alps. *Quat. Sci. Rev.* **2008**, *27*, 337–350. [[CrossRef](#)]
63. Plan, L. Factors controlling carbonate dissolution rates quantified in a field test in the Austrian alps. *Geomorphology* **2005**, *68*, 201–212. [[CrossRef](#)]
64. Häuselmann, P. Surface corrosion of an Alpine karren field: Recent measures at Innerbergli (Siebenhengste, Switzerland). *Int. J. Speleol.* **2008**, *37*, 107–111. [[CrossRef](#)]
65. Krklec, K.; Domínguez-Villar, D.; Braucher, R.; Perica, D.; Mrak, I. Morphometric comparison of weathering features on side by side carbonate rock surfaces with different exposure ages—A case from the Croatian coast. *Quat. Int.* **2017**, *494*, 275–285. [[CrossRef](#)]
66. Hantke, R. *Eiszeitalter*; Ott Verlag: Thun, Switzerland, 1980; Volume 2, p. 703.
67. Maisch, M. Zur Gletscher- und Klimageschichte des alpinen Spätglazials. *Geogr. Helv.* **1982**, *37*, 93–104. [[CrossRef](#)]
68. Jordi, U. *Glazialmorphologische und Gletschergeschichtliche Untersuchungen im Taminatal und im Rheintalabschnitt zwischen Flims und Feldkirch (Ostschweiz/Vorarlberg)*; Geographisches Institut der Universität Bern: Bern, Switzerland, 1986.
69. Weber, E.; Jordan, F.; Jeannin, P.-Y.; Vouillamoz, J.; Malard, A. Swisskarst project (NRP61): Towards a pragmatic simulation of karst spring discharge with conceptual semi-distributed model. The Flims case study (Eastern Swiss Alps). In Proceedings of the 9th Conference Limestone Hydrogeology, Besançon, France, 1–3 September 2011.
70. Hallet, B. A theoretical model of glacial abrasion. *J. Glaciol.* **1979**, *23*, 39–50. [[CrossRef](#)]
71. Ugelvig, S.V.; Egholm, D.L.; Anderson, R.S.; Iverson, N.R. Glacial Erosion Driven by Variations in Meltwater Drainage. *J. Geophys. Res. Earth Surf.* **2018**, *123*, 2863–2877. [[CrossRef](#)]
72. Dühnforth, M.; Anderson, R.S.; Ward, D.; Stock, G.M. Bedrock fracture control of glacial erosion processes and rates. *Geology* **2010**, *38*, 423–426. [[CrossRef](#)]
73. Krabbendam, M.; Glasser, N.F. Glacial erosion and bedrock properties in NW Scotland: Abrasion and plucking, hardness and joint spacing. *Geomorphology* **2011**, *130*, 374–383. [[CrossRef](#)]
74. Lane, T.P.; Roberts, D.H.; Rea, B.R.; Cofaigh, C.Ó.; Vieli, A. Controls on bedrock bedform development beneath the Ummannaq Ice Stream onset zone, West Greenland. *Geomorphology* **2015**, *231*, 301–313. [[CrossRef](#)]
75. Haeblerli, W.; Linsbauer, A.; Cochachin, A.; Salazar, C.; Fischer, U.H. On the morphological characteristics of overdeepenings in high-mountain glacier beds. *Earth Surf. Process. Landf.* **2016**, *41*, 1980–1990. [[CrossRef](#)]
76. MacGregor, K.R.; Anderson, R.S.; Anderson, S.P.; Waddington, E.D. Numerical simulations of glacial-valley longitudinal profile evolution. *Geology* **2000**, *28*, 1031–1034. [[CrossRef](#)]
77. Sugden, D.E.; John, B.S. *Glaciers and Landscape: A Geomorphological Approach*; Arnold: London, UK, 1976.
78. Evans, I.S. *Glacial Erosional Processes and Forms Mountain Glaciation and Glacier Geography*; The Geological Society: London, UK, 2008.

-
79. Evans, I.S. Glaciers, rock avalanches and the ‘buzzsaw’ in cirque development: Why mountain cirques are of mainly glacial origin. *Earth Surf. Process. Landf.* **2021**, *46*, 24–46. [[CrossRef](#)]
 80. Wirsig, C.; Ivy-Ochs, S.; Akçar, N.; Lupker, M.; Hippe, K.; Wacker, L.; Vockenhuber, C.; Schlüchter, C. Combined cosmogenic ^{10}Be , in situ ^{14}C and ^{36}Cl concentrations constrain Holocene history and erosion depth of Grueben glacier (CH). *Swiss J. Geosci.* **2016**, *109*, 379–388. [[CrossRef](#)]